We are IntechOpen,
the world's leading publisher of
Open Access books
Built by scientists, for scientists

4,800
Open access books available

122,000
International authors and editors

135M
Downloads

Our authors are among the

154
Countries delivered to

TOP 1%
most cited scientists

12.2%
Contributors from top 500 universities

CLARIVATE ANALYTICS
BOOK CITATION INDEX
INDEXED

WEB OF SCIENCE™

Selection of our books indexed in the Book Citation Index
in Web of Science™ Core Collection (BKCI)

Interested in publishing with us?
Contact book.department@intechopen.com

Numbers displayed above are based on latest data collected.
For more information visit www.intechopen.com

Dielectrophoresis for Manipulation of Bioparticles

Naga Siva K. Gunda and Sushanta K. Mitra
University of Alberta
Canada

1. Introduction

The objective of the present chapter is to provide a comprehensive description of dielectrophoresis (DEP), an electrokinetic technique, which has immense capability to manipulate bioparticles from micro- to nano-scale range. DEP is the movement of dielectric particles due to polarization effects in nonuniform electric fields (Pohl, 1978). The usual way of applying this technique is by flowing/placing the suspended particle solution on the planar microelectrode structures. The advancements in micro/nano fabrication techniques help in the development of such micro/nano electrode structures to generate the nonuniform electric field in DEP channels (Hughes, 2003). DEP assisted by such miniaturized electrodes have been used for separating, sorting, positioning, trapping, concentrating, and mixing (Gunda et al., 2009) of biomolecules such as cells, bacteria, virus, DNA and proteins (Basuray & Chang, 2010; Bunthawin et al., 2010; Church et al., 2009; Du et al., 2008; Ferrier et al., 2008; Gagnon et al., 2009; Hughes, 2003; Hwang et al., 2009; Jones, 1995; Lewpiriyawong et al., 2008; Lin & Yeow, 2007; Nguyen & Werely, 2006; Parikesit et al., 2008; Pohl, 1978; Wei et al., 2009; Yang et al., 2010; Zhu et al., 2010). These applications of DEP for manipulating such bioparticles has been further exploited in different fields namely drug delivery, food diagnostics, point of care analysis, biomedical, etc (Hughes, 2003).
The present chapter begins with brief description of DEP theory and mathematical modeling of DEP force field and spatial concentration distribution of particles inside the microchannel embedded with array of rectangular microelectrodes at the bottom. Then fabrication and experimental details of such DEP microfluidic device to manipulate bioparticles is discussed.

2. DEP Theory

DEP is manipulation of dielectric particles because of polarization effects under nonuniform direct current (DC) or alternating current (AC) electric fields (Pohl, 1978). The net force created with DEP generates momentum in the particles. Particle movement towards regions of high electric field intensities is called positive DEP and occurs when the interior of the particle is more permissive to the field. The opposite effect is the movement towards lower electric field intensities called negative DEP, when the exterior is more permissive (Hughes, 2003; Jones, 1995; Pohl, 1978). The frequency at which the DEP effect changes from positive DEP to negative DEP or negative DEP to positive DEP is called crossover frequency (Jones, 1995; Pohl, 1978). The DEP force depends on both the gradient of the electric field and electrical properties such as permittivity and conductivity of the particle and medium. It is important to note that the force due to DEP is based on the gradient of electric field and not on the absolute

value of electric field at any point. Analysis of movement of the particles in a nonuniform electric field needs an accurate knowledge of the electric field distribution in the system. Different electrode geometries and arrangements are used to produce nonuniform electric field. They are polynomial electrodes, castellated electrodes, interdigited electrodes, and array of electrodes. Each arrangement has its own advantages and disadvantages. Bioparticles can be any shape like spherical, oblate, prolate, disc, rod, etc., with dimensions ranging from micron to nano-scale. Assuming arbitrary shape of bioparticles, here we are providing the time averaged dielectrophoretic force $\mathbf{F}_{DEP}$ acts on any arbitrary shaped particle due to stationary wave nonuniform AC electric field. It is derived with slight modification of $\mathbf{F}_{DEP}$ acting on spherical particles provided by Pohl (1978)

$$\mathbf{F}_{DEP} = \frac{3}{2}(vol)\varepsilon_m Re[K(\omega)]\nabla(\mathbf{E}\cdot\mathbf{E}) \tag{1}$$

where (vol) is the volume of particle, ε_m is the permittivity of medium, $Re[K(\omega)]$ is real part of Clausius-Mossotti (CM) factor and $\mathbf{E}$ is the applied electric field vector. CM factor for any arbitrary shaped particle is given as (Yang & Lei, 2007)

$$K(\omega) = \frac{1}{3}\frac{(\varepsilon'_p - \varepsilon'_m)}{\varepsilon'_m + A_\alpha(\varepsilon'_p - \varepsilon'_m)} \tag{2}$$

where A_α is the depolarization factor, subscript α relates to axis of the particle x or y or z and ε'_p and ε'_m are complex permittivities of particle and medium, respectively. They are given as

$$\varepsilon'_p = \varepsilon_p - j\frac{\sigma_p}{\omega} \tag{3}$$

$$\varepsilon'_m = \varepsilon_m - j\frac{\sigma_m}{\omega} \tag{4}$$

where ε_p and ε_m are permittivity of particle and medium respectively, σ_p and σ_m are conductivity of particle and medium respectively, ω is angular frequency of the applied field and $j = \sqrt{-1}$. Depolarization factor for the CM factor varies according to the shape of the particle which leads to change in DEP force. Yang & Lei (2007) reported the calculation of depolarization factor for ellipsoidal, oblate and prolate spheroid shapes. The sum of different axis depolarization factors for a particle should be unity. Considering a, b, and c as dimensions of the particles in the x, y, and z-axis directions respectively, the depolarization factors are given as

For Sphere ($a = b = c$):

$$A_x = A_y = A_z = \frac{1}{3} \tag{5}$$

For Oblate spheroid ($a = b > c$):

$$A_x = A_y = \frac{a^2c}{2(a^2 - c^2)}\left[\frac{\pi/2}{\sqrt{(a^2 - c^2)}} - \frac{c}{a^2}\right] \tag{6}$$

$$A_z = 1 - 2A_x = 1 - 2A_y \tag{7}$$

For Prolate spheroid ($a > b = c$):

$$A_x = \frac{b^2}{2a^2e^3}\left[\ln(\frac{1+e}{1-e}) - 2e\right] \tag{8}$$

$$A_y = A_z = \frac{(1 - A_x)}{2} \qquad (9)$$

where eccentricity (e) is given as $\sqrt{(1 - \frac{b^2}{a^2})}$. It is observed that CM factor varies with respect to axis of the particle. But in the microchannel, the direction of DEP force acting on the particle is arbitrary. Hence, average CM factor is considered for the particle for calculating DEP force. From Eqn. (1), it is observed that DEP force becomes less effective for small particles, mainly with molecular sizes and submicron particles where thermal effects are dominant. Most of the conventional DEP experiments demonstrated the response of particles with the change in frequency of the applied electric field to decide the crossover frequencies (Castellarnau et al., 2006). This crossover frequencies can be calculated from complex CM factor $K(\omega)$. If $Re[K(\omega)] \geq 0$, positive DEP occurs, otherwise negative DEP occurs. Theoretically, $Re[K(\omega)]$ varies from -0.5 to +1 (Jones, 1995; Pohl, 1978). The crossover frequency for any arbitrary shaped particle is given as

$$f_c = \frac{1}{2\pi} \sqrt{\frac{(\sigma_m - \sigma_p)[\sigma_m + A_\alpha(\sigma_p - \sigma_m)]}{(\varepsilon_p - \varepsilon_m)[\varepsilon_m + A_\alpha(\varepsilon_p - \varepsilon_m)]}} \qquad (10)$$

It is observed that f_c can be calculated only when $\frac{(\sigma_m - \sigma_p)}{(\varepsilon_p - \varepsilon_m)} > 0$. If $\varepsilon_p = \varepsilon_m$, f_c will tend to ∞, and practically, it is not possible to apply such frequency for observing the two types of DEP effects. Bioparticles might be made up of two or three different layers with different conductivity and permittivity values. In such cases, the DEP force shown in Eqn. (1) is still valid, if ε'_p is replaced with effective complex permittivity ε'_{peff}. For a two layered particle where particle p is surrounded with another layer 2, the effective complex permittivity ε'_{peff} as given by (Jones, 1995; Yang & Lei, 2007)

$$\varepsilon'_{peff} = \varepsilon'_{p2} \left[\frac{\varepsilon'_p + t_\alpha(\varepsilon'_p + \varepsilon'_{p2})/q_\alpha}{\varepsilon'_{p2} + t_\alpha(\varepsilon'_p + \varepsilon'_{p2})/q_\alpha} \right] \qquad (11)$$

where t_α is the thickness of particle layer 2 along x, y, and z-axis, q_α = a, b, and c for α = x, y, and z, respectively and ε'_{p2} is the complex permittivity of hydration layer which can be written as

$$\varepsilon'_{p2} = \varepsilon_{p2} - j\frac{\sigma_{p2}}{\omega} \qquad (12)$$

where ε_{p2} and σ_{p2} are permittivity and conductivity of layer 2, respectively. The interested reader can refer to Jones (1995) or Yang & Lei (2007) for calculating effectives complex permittivity of three layered particles.

Mathematical modeling

The governing equations for dielectrophoretic transport of particles in aqueous solution require the Laplace equation for calculating electric field distributions in a system, Navier-Stokes equation for calculating fluid velocity distribution in a system and convection-diffusion-migration equation for determining the particles distribution. In the present study, the following assumptions are made: (i) the aqueous solution containing particles flowing through the microchannel are at steady state, incompressible and behave like Newtonian fluids; (ii) no chemical reactions take place between the particles or between the particles and walls of the channel; (iii) Electric double-layer, van der Waals and electrothermal effects are neglected.

2.1 Laplace equation

The electric field distribution in the system created by AC signal is described by the Laplace equation (Masliyah & Bhattacharjee, 2006)

$$\nabla^2\phi = 0 \tag{13}$$

where ϕ is the applied electric potential. Solving Eqn.(13) with appropriate boundary conditions will provide the potential distribution in the computational domain. This potential distribution is used to calculate the DEP force acting on particles.

2.2 Navier-Stokes equation

For an incompressible flow at low Reynolds number, the steady state continuity and Navier-Stokes equations neglecting inertial and body forces are given by,

$$\nabla \cdot \mathbf{u} = 0 \tag{14}$$

$$\nabla p = \mu\nabla^2\mathbf{u} \tag{15}$$

2.3 Convection-diffusion-migration equation

The steady state concentration distribution of particles in an aqueous solution with no chemical reactions can be given by convection-diffusion-migration equation as (Masliyah & Bhattacharjee, 2006)

$$\nabla\cdot(\mathbf{u}C) = \nabla\cdot(\mathbf{D}\cdot\nabla C) - \nabla\cdot\left(\frac{\mathbf{D}\cdot\mathbf{F}_{mig}}{k_BT}C\right) \tag{16}$$

where $\mathbf{u}$ is the medium velocity vector, C is the concentration of particles, $\mathbf{D}$ is diffusion coefficient tensor, $\mathbf{F}_{mig}$ is the migrational force vector on particles due to DEP, k_B is Boltzmann constant $(1.3806503 \times 10^{-23}m^2kgs^{-2}K^{-1})$ and T is the ambient temperature. The first term of Eqn. (16) represents the transport due to convection, the second term is the transport due to diffusion, and the third term indicates the transport due to migration. Since the interactions between particles are neglected in the assumptions, diffusion tensor $\mathbf{D}$ can be simplified as the Stokes-Einstein diffusion coefficient D_∞,

$$D_\infty = \frac{k_BT}{f} \tag{17}$$

where $f = 12A_p\mu/l_c$. Here f is the friction factor, A_p is the projected area of the particle, μ is the dynamic viscosity of medium, and l_c is the characteristic length of particle. Both A_p and l_c depend on the shape of the particle and the direction of flow over it. The particle migration velocity for steady state problem can be given as

$$\mathbf{u}_{mig} = \frac{\mathbf{D}\cdot(\mathbf{F}_{mig})}{k_BT} = \frac{\mathbf{F}_{mig}}{f} \tag{18}$$

Combining and rearranging Eqs. (16-18) gives the following modified steady state convection-diffusion-migration equation

$$\mathbf{u}_{tot}\nabla C = D_\infty\nabla^2 C \tag{19}$$

where $\mathbf{u}_{tot} = \mathbf{u} + \mathbf{u}_{mig}$. Solving Eqn. (19) with appropriate boundary conditions will provide the spatial concentration distribution of particles in the computational domain. This concentration distribution is used to check the effectiveness of applying DEP force for manipulating submicron particles.
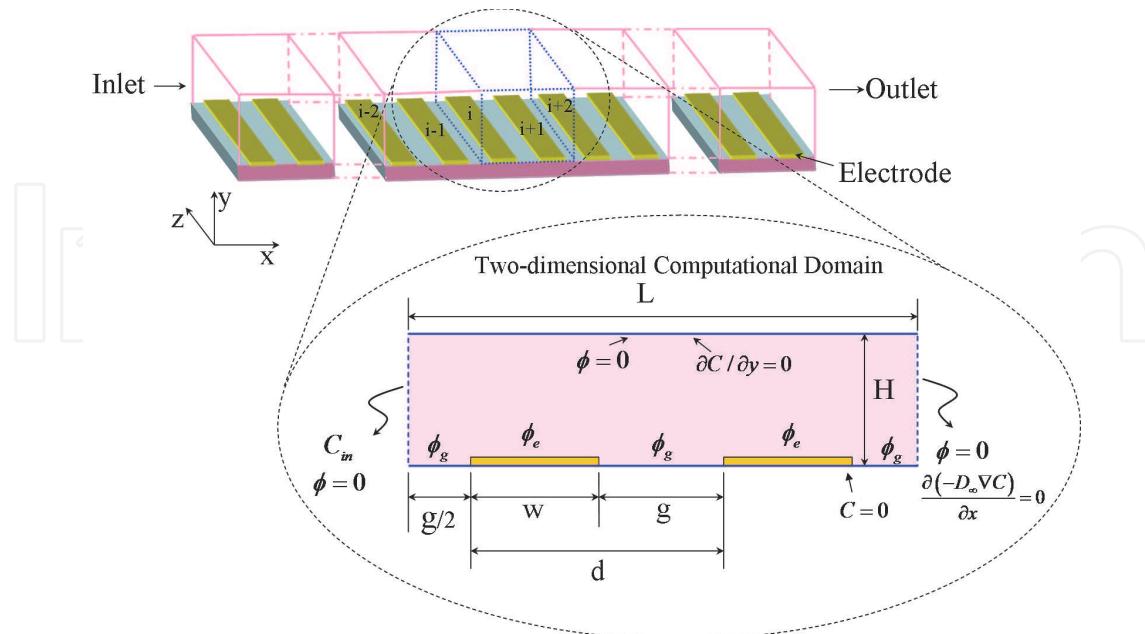
2.4 Computational domain

Fig. 1. Schematic view of DEP microfluidic device considered for manipulating the particles. Enlarged view shows the two-dimensional computational domain considered for analysis

Figure 1 depicts the schematic view of the DEP microfluidic system considered for manipulation of microparticles under DEP effects. The device has infinite number of electrodes ($-\infty,...,-3,-2,-1,0,1,2,3,...,\infty$) on the bottom surface of the microchannel. The enlarged view in Fig.1 shows the two-dimensional computational domain considered for numerical and analytical analysis. Here L is the length of channel considered for computational domain and H is the height. The bottom surface is embedded with array of parallel rectangular microelectrodes of width w and gap g in between the electrodes. The parameter d represents the sum of electrode width w and gap g and ϕ represents the applied electric potential. The notation i and $(i+1)$ represents the ith and $(i+1)^{th}$ electrodes, respectively. Appropriate boundary conditions to solve the above governing equations is also provided in the Fig.1. The remaining boundaries are kept insulated/symmetry for convection-diffusion-migration equation, zero charge/symmetry for Laplace equation and no-slip boundary conditions at walls for Navier-Stokes equation.

2.5 Solution methodology

The procedure for solving the concentration field is divided into three steps: (i) evaluating the electric field distribution in the system using Eqn. (13); (ii) evaluating the flow field velocity distribution in the system using Eqns. (14) and (15); (iii) evaluating the particle spatial concentration distribution using Eqn. (19). Step (i) and (ii) are solved independently, because electrical body forces in the system are neglected. The solution obtained in step (i) is used to find the DEP force. Solutions obtained in step (i) and step (ii) are incorporated into the Eqn. (19) to calculate concentration distribution of particles in the system under negative DEP effects.

The potential distribution is solved analytically as well as numerically. The analytical expression for potential, electric field and DEP force distributions in a microchannel containing parallel array of electrodes at the bottom surface has been already reported

in many research papers on the basis of charge density method (Wang et al., 1993), Green's theorem (Clague & Wheeler, 2001; Molla & Bhattacharjee, 2005a;b; Wang et al., 1996), conformal mapping (Manuel & Clague, 2000) and Fourier series (Morgan et al., 2001). The closed form solutions are also developed for electric field and DEP forces by Morgan et al. (2001) and Chang et al. (2003). Wang et al. (1996) compared the analytical solution from Green's Theorem based method with charge density method, whereas Green et al. (2002) compared the analytical solution from Fourier series method with numerical solution solved by finite element method. Clague & Wheeler (2001), and Crews et al. (2001) studied the effect of electrode dimensions, channel height and applied voltage on gradient of squared electric field. Molla & Bhattacharjee (2005a;b) compared the Green's theorem based analytical and finite element based numerical solutions as well as studied the effect of applied voltages and frequencies on DEP force. In the present study, a simple and modified analytical expressions for electric field and gradient of squared electric field squared are derived based on Green's theorem method. In addition, a mesh independent numerical solution using finite element method is also solved. These analytical and numerical solutions are compared with Fourier series method (Morgan et al., 2001) and closed form solutions (CFS) by Morgan et al. (2001) and Chang et al. (2003).

Here, the analytical expressions for potential, electric field and gradient of squared electric field using Green's theorem method is derived. The potential and electric field distributions along the length of the electrodes are uniform for array of parallel rectangular electrodes. Therefore, the in-plane dimension of the system is neglected here. The Laplace equation for two-dimensional system as shown in Fig.1 is solved. Sinusoidal voltage of phase difference $2\pi/n$ and angular frequency ω are applied on the electrodes for producing nonuniform electric field. For particles under stationary wave DEP, value of n will be 2 (Clague & Wheeler, 2001; Molla & Bhattacharjee, 2005b; Wang et al., 1996). The analytical solution for the Laplace equation using Green's theorem for upper half-space, $y \geq 0$ is given as

$$\phi(x,y) = \frac{y}{2\pi} \int \frac{\phi dx_0}{[(x - x_0)^2 + y^2]} \tag{20}$$

where x_0 represents the point in x direction on the electrode plane and ϕ represents the surface potential on the electrode plane. The potential distribution is solved by piecewise integration of Eqn. (20) with surface potential boundary conditions on electrode plane. Assuming the linear variation of surface potential at gap between the electrodes (Chang et al., 2003; Clague & Wheeler, 2001; Crews et al., 2001; Green et al., 2002; Molla & Bhattacharjee, 2005a;b; Morgan et al., 2001; Wang et al., 1996), the surface potential boundary conditions on electrodes and gap between electrodes are given as

$$\phi_e(x_0) = \phi cos \left(\omega t + \frac{2\pi i}{n} \right) \tag{21}$$

$$\phi_g(x_0) = \phi \left\{ S \left[x_0 - (id + \frac{w}{2}) \right] + cos \left(\omega t + \frac{2\pi i}{n} \right) \right\} \tag{22}$$

where $S = \{cos(\omega t + 2\pi(i+1)/n) - cos(\omega t + 2\pi i/n)\}/g$, the limits of x_0 for electrodes varies from $id - w/2$ to $id + w/2$ and the limits of x_0 for gap between the electrodes varies from $id + w/2$ to $(i+1)d - w/2$. Here i is the ith electrode and varies from $-\infty$ to $+\infty$. Substituting the Eqns.(21) and (22) into Eqn. (20) and integrating yields the potential distribution expression

as

$$\phi(x, y \geq 0) = \frac{1}{\pi} \sum_{i=-\infty}^{\infty} \left\{ -\phi_e(x) \left(tan^{-1} \left[\frac{x - q_i}{y} \right] - tan^{-1} \left[\frac{x - p_i}{y} \right] \right) \right\}$$

$$+ \frac{1}{\pi} \sum_{i=-\infty}^{\infty} \left\{ +\phi_g(x) \left(tan^{-1} \left[\frac{x - q_i}{y} \right] - tan^{-1} \left[\frac{x - p_{i+1}}{y} \right] \right) \right. \tag{23}$$

$$\left. - \frac{Sy}{2} \left(ln \left[(x - q_i)^2 + y^2 \right] - ln \left[(x - p_{i+1})^2 + y^2 \right] \right) \right\}$$

where $p_i = id - w/2$, $q_i = id + w/2$, and $p_{i+1} = (i+1)d - w/2$. Electric field distribution in the system can be calculated from the above potential distribution expression using $\mathbf{E} = -\nabla \phi$. The term $\nabla(\mathbf{E} \cdot \mathbf{E})$ in Eqn. (1) can be expressed for a two-dimensional computational domain as follows:

$$\frac{\partial}{\partial x}(\mathbf{E} \cdot \mathbf{E}) = 2(E_x \frac{\partial E_x}{\partial x} + E_y \frac{\partial E_y}{\partial x}) \tag{24}$$

$$\frac{\partial}{\partial y}(\mathbf{E} \cdot \mathbf{E}) = 2(E_x \frac{\partial E_x}{\partial y} + E_y \frac{\partial E_y}{\partial y}) \tag{25}$$

where E_x is electric field in the x direction, E_y is electric field in the y direction.
The expressions E_x, E_y, $\partial E_x / \partial x$, $\partial E_y / \partial x$, $\partial E_x / \partial y$ and $\partial E_y / \partial y$ are derived by differentiating the potential distribution function given in Eqn. (23). The expressions derived for potential, electric field in x and y directions are similar to the Wang et al. (1996), Clague & Wheeler (2001) and Molla & Bhattacharjee (2005a;b) with different notation. Here the simplified and modified expressions are provided. The following expressions can be used to calculate the DEP forces by substituting into Eqn. (1)

$$E_x = \frac{1}{\pi} \sum_{i=-\infty}^{\infty} \left\{ \phi_e(x) y \left(\frac{1}{y^2 + (x - q_i)^2} - \frac{1}{y^2 + (x - p_i)^2} \right) \right\}$$

$$+ \frac{1}{\pi} \sum_{i=-\infty}^{\infty} \left\{ -\phi_g(x) y \left(\frac{1}{y^2 + (x - q_i)^2} - \frac{1}{y^2 + (x - p_{i+1})^2} \right) \right.$$

$$+ Sy \left(\frac{x - q_i}{y^2 + (x - q_i)^2} - \frac{x - p_{i+1}}{y^2 + (x - p_{i+1})^2} \right) \tag{26}$$

$$\left. - S \left(tan^{-1} \left[\frac{x - q_i}{y} \right] - tan^{-1} \left[\frac{x - p_{i+1}}{y} \right] \right) \right\}$$

$$E_y = \frac{1}{\pi} \sum_{i=-\infty}^{\infty} \left\{ -\phi_e(x) \left(\frac{x - q_i}{y^2 + (x - q_i)^2} - \frac{x - p_i}{y^2 + (x - p_i)^2} \right) \right\}$$

$$+ \frac{1}{\pi} \sum_{i=-\infty}^{\infty} \left\{ +\phi_g(x) \left(\frac{x - q_i}{y^2 + (x - q_i)^2} - \frac{x - p_{i+1}}{y^2 + (x - p_{i+1})^2} \right) \right.$$

$$+ Sy^2 \left(\frac{1}{y^2 + (x - q_i)^2} - \frac{1}{y^2 + (x - p_{i+1})^2} \right) \tag{27}$$

$$\left. + \frac{S}{2} \left(ln \left[(x - q_i)^2 + y^2 \right] - ln \left[(x - p_{i+1})^2 + y^2 \right] \right) \right\}$$

$$\frac{\partial E_x}{\partial x} = -\frac{\partial E_y}{\partial y}$$

$$= \frac{1}{\pi} \sum_{i=-\infty}^{\infty} \left\{ -2\phi_e(x)y \left(\frac{x-q_i}{[y^2+(x-q_i)^2]^2} - \frac{x-p_i}{[y^2+(x-p_i)^2]^2} \right) \right\}$$

$$+ \frac{1}{\pi} \sum_{i=-\infty}^{\infty} \left\{ +2\phi_g(x)y \left(\frac{x-q_i}{[y^2+(x-q_i)^2]^2} - \frac{x-p_{i+1}}{[y^2+(x-p_{i+1})^2]^2} \right) \right.$$

$$+ Sy \left(\frac{y^2-(x-q_i)^2}{[y^2+(x-q_i)^2]^2} - \frac{y^2-(x-p_{i+1})^2}{[y^2+(x-p_{i+1})^2]^2} \right)$$

$$\left. -2Sy \left(\frac{1}{y^2+(x-q_i)^2} - \frac{1}{y^2+(x-p_{i+1})^2} \right) \right\} \qquad (28)$$

$$\frac{\partial E_x}{\partial y} = \frac{\partial E_y}{\partial x}$$

$$= \frac{1}{\pi} \sum_{i=-\infty}^{\infty} \left\{ -\phi_e(x) \left(\frac{y^2-(x-q_i)^2}{[y^2+(x-q_i)^2]^2} - \frac{y^2-(x-p_i)^2}{[y^2+(x-p_i)^2]^2} \right) \right\}$$

$$+ \frac{1}{\pi} \sum_{i=-\infty}^{\infty} \left\{ +\phi_g(x) \left(\frac{y^2-(x-q_i)^2}{[y^2+(x-q_i)^2]^2} - \frac{y^2-(x-p_{i+1})^2}{[y^2+(x-p_{i+1})^2]^2} \right) \right.$$

$$-2Sy^2 \left(\frac{x-q_i}{[y^2+(x-q_i)^2]^2} - \frac{x-p_{i+1}}{[y^2+(x-p_{i+1})^2]^2} \right) \qquad (29)$$

$$\left. +2S \left(\frac{x-q_i}{y^2+(x-q_i)^2} - \frac{x-p_{i+1}}{y^2+(x-p_{i+1})^2} \right) \right\}$$

Analytical methods give exact solution to the potential and electric field distributions in the system as well as DEP force on the particles. This analytical method is only applicable to simplified geometries (mainly two-dimensional) like infinite array of parallel electrodes. However, most of the applications, electrode geometries and layouts are different and not possible to simplify as two-dimensional models. Solving the two-dimensional convection-diffusion-migration equation by analytical methods is a tedious process due to elliptical nature of equation. Therefore, numerical method is implemented to obtain approximate solutions for electric field and particle concentration distributions in the system. The governing equations and the boundary conditions described earlier are implemented in a finite element based software COMSOL Multiphysics version 3.5a (COMSOL, Inc., Burlington, MA, USA), to study the dielectrophoretic behavior of microparticles. To obtain the numerical solution, only two electrodes are used for simulations instead of array of electrodes as it is periodic in nature (as shown in Fig.1). The two-dimensional computational domain is discretized with quadrilateral elements. The electrode edges are discretized with finer elements to capture the effect of high intensity electric field. The model uses Lagrange-quadratic elements for calculating parameters inside the domain like electric potential, electric field, etc. The structured (mapped) mesh scheme is used to discretize the computational domain. The simultaneous linear equations produced by the finite element method are solved using direct elimination solver (PARDISO). A mesh independent finite element solution is achieved with around $12,000$ elements. The convection-diffusion-migration model is solved with small artificial isotropic diffusion ($=$ 0.05) to improve the convergence and to reduce the oscillations in concentration profile (Molla & Bhattacharjee, 2007).

2.6 Modeling results

Results for the dielectrophoretic behavior of the bioparticles in aqueous solution are presented in this section. All the results shown for the case when the width of the electrode is equal to gap between the electrodes ($W = G$). Similar results are observed for other electrode configurations ($W < G$ and $W > G$), which are not described here for the sake of brevity. Thickness of the electrodes is assumed to be very small as compared to the height of channel and hence neglected in the simulations. The height of the channel is three times the width of electrodes ($H = 3W$).
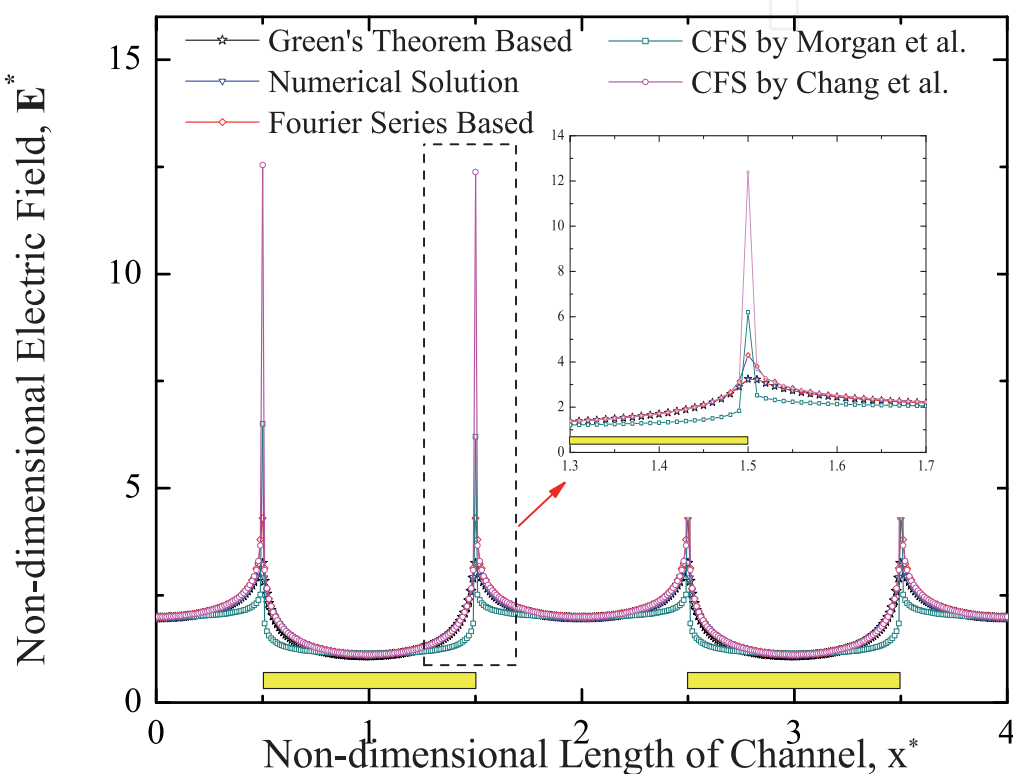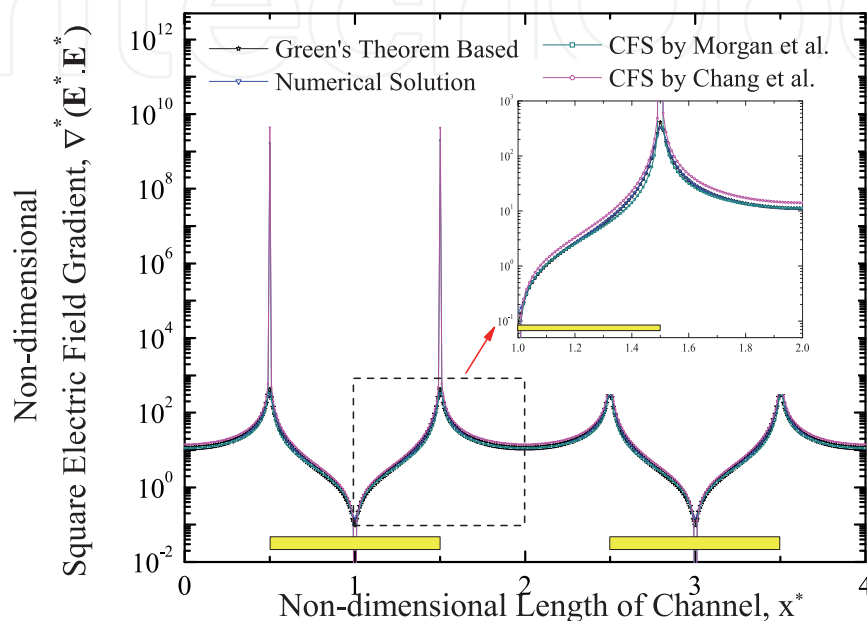

Fig. 2. Comparison of non-dimensional electric field along the length of channel near the electrodes for different solution methods

Figure 2 shows the comparison of non-dimensional electric field along the length of channel near the electrodes for Green's theorem based analytical solution, Fourier series based analytical solution (Morgan et al., 2001), finite element based numerical solution, CFS by Morgan et al. (2001) and CFS by Chang et al. (2003). The horizontal axis in this figure shows the non-dimensional length of the channel (x^*), whereas vertical axis shows the non-dimensional electric field ($\mathbf{E}^*$). The different symbols in the figure indicates the different solution methods. The electric field is maximum at the edges of the electrodes and minimum else where. But the magnitude of the electric field at the center of the electrode is very less than the electric field at the mid point of the gap between the electrodes. The excellent agreement is observed between Green's theorem based analytical solution and finite element based

numerical solution. However, slight discrepancies are identified at the edge of the electrode for Green's theorem based/numerical solution with Fourier series based analytical solution and CFS by Chang et al. The peak magnitude for non-dimensional electric field is observed for CFS by Chang et al. compared with other solution methods. CFS by Morgan et al. (2001) has slight flat profile along the electrodes/gap between electrodes compared to semi circular curved profile of non-dimensional electric field for other solution methods.

Fig. 3. Comparison of non-dimensional squared electric field gradient along the length of channel near the electrodes for different solution methods

As discussed earlier, DEP force depends on the volume of particle, real part of the CM factor and the gradient of squared electric field. Since the effect of presence of microparticles on electric field is neglected, gradient of squared electric field is independent of shape, size, and properties of particles. Hence, the variation of squared electric field gradient along the length of channel and height of the channel is studied. Figure 3 illustrates the comparison of non-dimensional squared electric field gradient with respect to length of channel near the electrode plane for Green's theorem-based analytical solution, numerical solution based on COMSOL, CFS by Morgan et al. (2001) and CFS by Chang et al. (2003). The horizontal axis in this figure shows the non-dimensional length of the channel (x^*) and vertical axis shows the non-dimensional squared electric field gradient ($\nabla^*(\mathbf{E}^* \cdot \mathbf{E})^*$). The different solution methods are indicated with different symbols in Fig. 3. The results show that the squared electric field gradient is maximum at the edges of the electrodes and minimum elsewhere. The magnitude of non-dimensional squared electric field gradient is in the range of 10^{-1} to 10^{10} for an applied electric potential of $\phi^* = 1$. The attraction or repulsion of particles can be achieved significantly due to large amount of electric field at the edges of the electrodes. The variation profile of non-dimensional squared electric field is almost matches with that of Green's theorem-based solution, numerical solution, and CFS by Morgan et al. (2001) and

Chang et al. (2003). The Fourier series-based solution is not compared here due to some large discrepancies with other solution methods. The excellent agreement is identified with Green's theorem-based solution and numerical solution, whereas some slight difference in non-dimensional squared electric field gradient is observed along the length of the channel (except the edges of electrode) with other solution methods. CFS by Chang et al. (2003) and Morgan et al. (2001) provide the maximum non-dimensional squared electric field gradient at the edges of the electrode compared to that of Green's theorem method and finite element method.
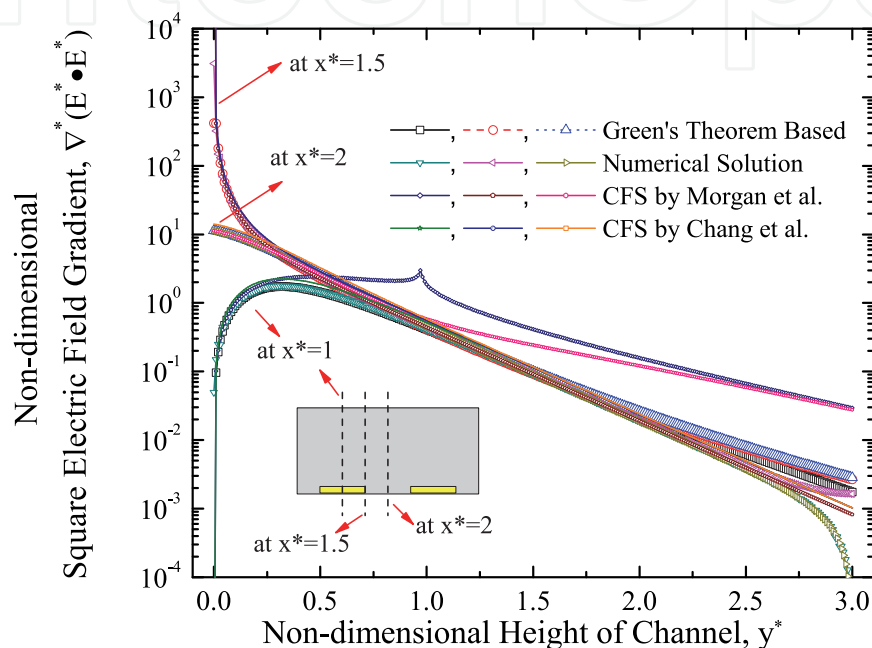
Fig. 4. Comparison of non-dimensional squared electric field gradient along the height of channel at edge of the electrode, mid point of the electrode and mid point of gap between the electrodes for different solution methods

Figure 4 depicts the comparison of non-dimensional squared electric field gradient with respect to the height of channel at electrode edge, mid point of electrode and mid point of gap between the electrodes with different solution methods. The horizontal axis in this figure shows the non-dimensional height of the channel (y^*) whereas vertical axis shows the non-dimensional squared electric field gradient ($\nabla^*(\mathbf{E}^* \cdot \mathbf{E})^*$). The non-dimensional squared electric field gradient decays exponentially along the height of channel at the edges of the electrodes. At mid point of electrodes, the squared electric field gradient increases exponentially $y^* = 0.32$ and then linearly decreased along the height of channel. The linear decaying of squared electric field is observed at the mid point of gap between the electrodes. At the height $y^* = 1.25$, the gradient of squared electric field is constant throughout the channel length and magnitude is decreased along the height of channel. This decides the effectiveness of DEP force in the channel. The profiles for variation of non-dimensional squared electric field gradient with different solution methods are matched for all the cases. There is some discrepancy with profiles along the height of channel at mid point of electrodes

for Green's theorem-based solution or numerical solution with CFS by Morgan et al. (2001) and Chang et al. (2003).
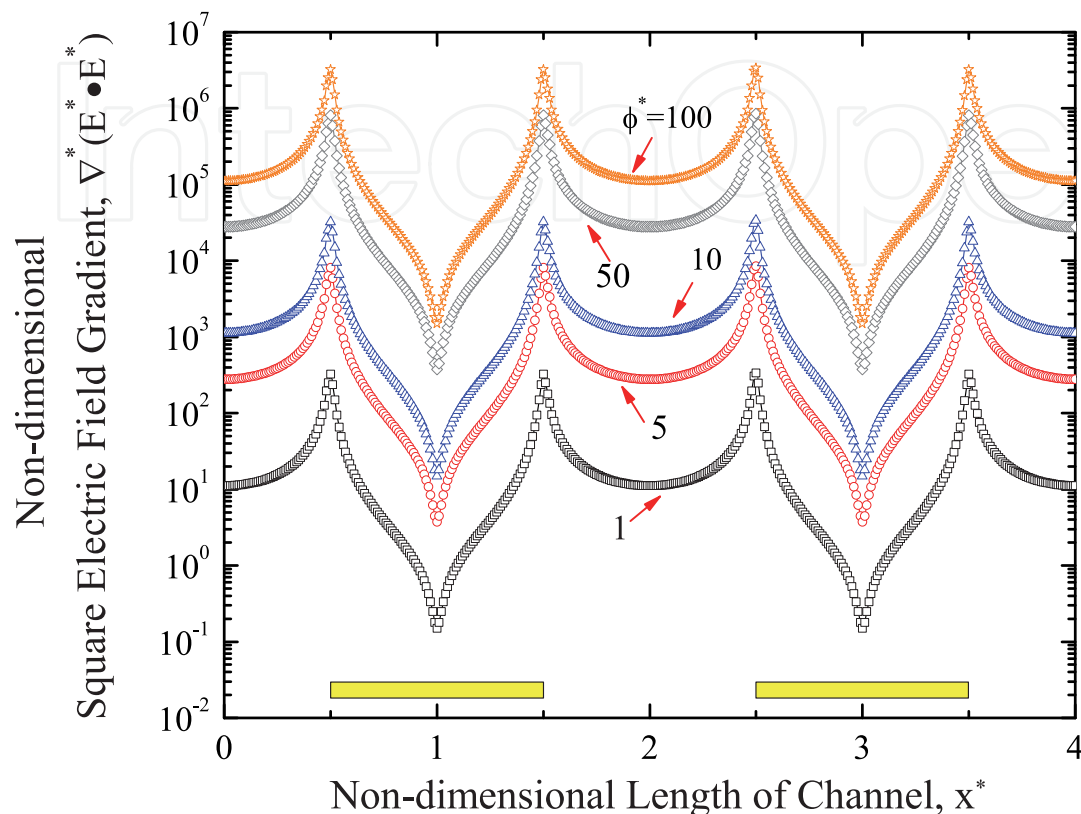

Fig. 5. Comparison of non-dimensional squared electric field gradient along the length of channel near the electrodes for different non-dimensional applied voltages

Figure 5 shows the dependence of non-dimensional squared electric field gradient on applied voltage along the length of channel near the electrodes. The horizontal axis in this figure shows the non-dimensional length of the channel (x^*), whereas vertical axis represents the non-dimensional gradient of the squared electric field. Different symbols indicate the different voltages in the figure. It is observed that squared electric field gradient is directly proportional to the applied voltage. The magnitude of peak non-dimensional squared electric field gradient is increased from 3×10^2 to 3×10^6 for an increase in non-dimensional applied voltage (ϕ^*) from 1 to 100, respectively.

Figure 6(a) and 6(b) shows the comparison of DEP velocity under positive and negative DEP effects, respectively. Arrows in figures indicate the direction of particles movement due to DEP force. The length of the arrow does not indicate the magnitude of the DEP velocity. Contours in the figure indicate the constant DEP velocities along the curves. In Fig. 6(a), converging of arrows at electrode edges indicate the collection of particles in that area, which can be used as concentration regions (or collectors). In Fig. 6(b), the direction of the particle movement has changed and the particles are being repelled from the electrode. As this is a closed channel, the particles are collecting at the top wall of the channel and at a position
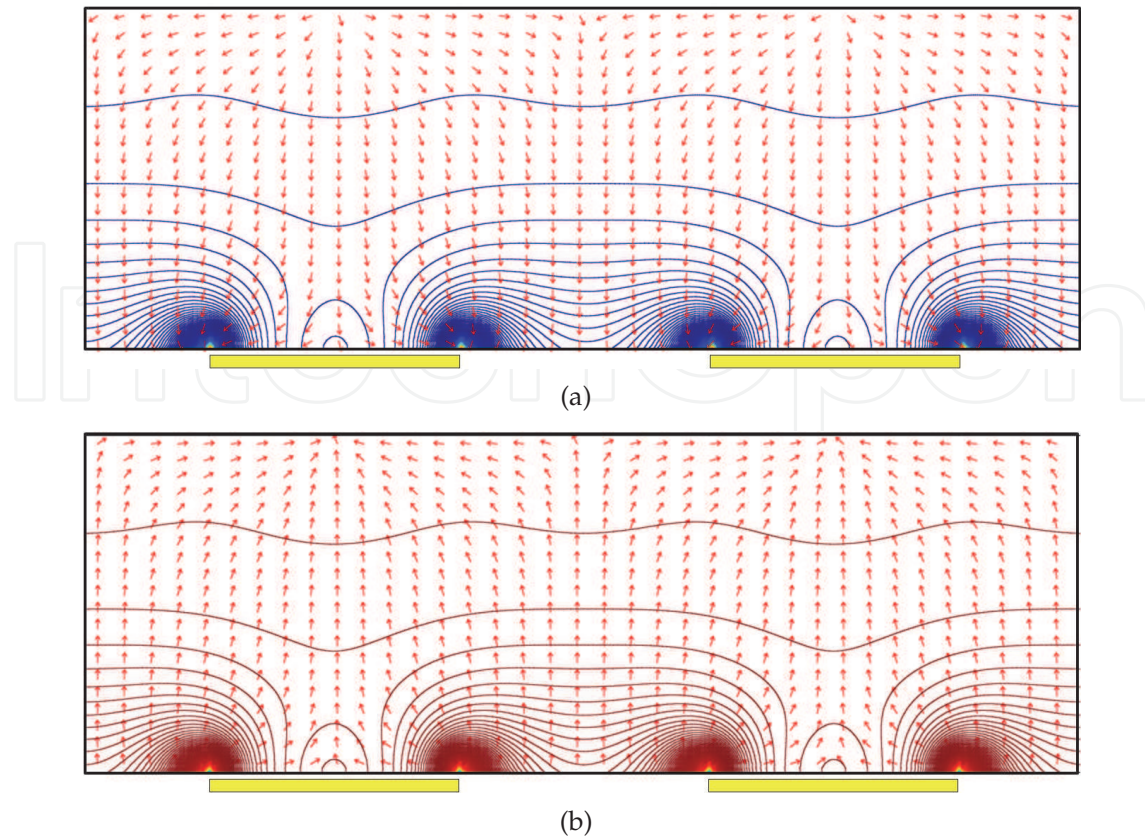
(a)

(b)

Fig. 6. Comparison of DEP velocity contour and arrow plots; (a) under positive DEP effect (b)under negative DEP effect

parallel to the mid-point of the electrode. The region where the particles are collecting is called concentrating regions.
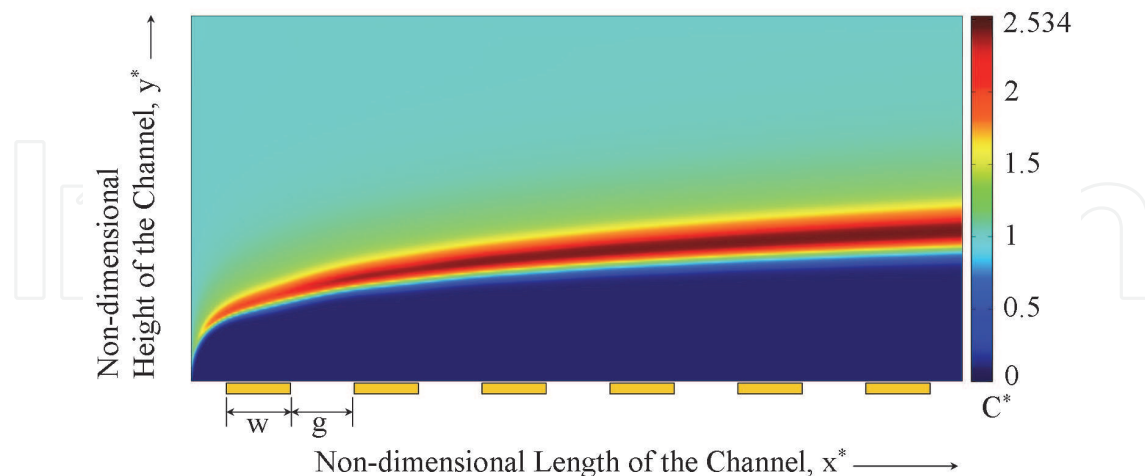

Fig. 7. Variation of mass concentration of the particles inside the microchannel under the influence of DEP and flow field along the channel

Figure 7 shows the variation of non-dimensional concentration of particles inside the microchannel. The particles are levitated to certain height due to repulsive DEP forces. This analysis is applied to myoglobin (Gunda & Mitra, 2009; 2010b) to study the behavior of

myoglobin in microchannel. In their study, a channel of 400 nm length and 300 nm height with 100 nm width electrodes and 100 nm gap is utilized to create nonuniformities in the electric field gradients. Maximum concentration distribution of the myoglobin was found at 240 nm, the channel height from the bottom wall under 10 Vpp, and 1 kHz AC voltage and frequency respectively. Both, positive and negative DEP effects were observed at 50 MHz and 1 kHz AC frequency respectively (Gunda & Mitra, 2009; 2010b).

3. Materials and methods

DEP microfluidic device can be fabricated using glass, PDMS and silicon materials. Experimental details of fabrication of channels and microelectrodes on PDMS and glass materials, respectively can be found at Gunda et al. (n.d.). In this chapter, we are providing the fabrication of DEP chip with two glass substrates.

Fabrication of DEP microfluidic device with two glass substrates with a network of microchannels, fluidic and electrical ports in top substrate and different set of microelctrodes in bottom substrates is described in this section. Initially, the layout of microelectrode configuration (rectangular array of electrodes) and microchannel are designed with the L-Edit MEMS Design software (MemsPRO v6, Tanner Research, Inc., CA) and then exported to Laser Pattern Generator (Heidelberg DWL-200, Heidelberg Instruments, Germany) for fabricating the chrome masks. These chrome masks are used in the photolithography process to transfer the structures on the glass substrates.

3.1 Fabrication of microelectrodes

Fabrication of microelectrodes on glass substrate is described in this section. Piranha (H_2SO_4:H_2O_2 of 4:1 by volume)cleaned borofloat glass wafer (Paragon Optical Company, Inc., PA) of $4\ in \times 4\ in$ and 1.1 mm thick is taken and a layer of 40 nm chromium and 200 nm gold sequentially deposited using planar magnetron sputtering system. The gold coated glass wafer is then spin-coated with a layer of $1-2\ \mu m$ positive photoresist(PPR)(HPR 504, Fujifilm Electronic Materials, Inc., Arizona) using Solitec resist spinner (Model 5110-CD, Solitec Wafer Processing, Inc., CA). Then, the PPR coated wafer is soft-baked at 110 ^oC for 90 s on a Solitec vacuum hot plate (Solitec Wafer Processing, Inc., CA). Using mask aligner, the spin-coated wafer is exposed to UV illumination (350-400 nm) through chrome mask for $2-3\ s$ to transfer the electrode structures on PPR. The wafer is then developed using PPR developer (HPRD 429, Fujifilm Electronic Materials, Inc., Arizona) for $20-30\ s$. Later, gold and chromium are etched using gold etchant ($KI + I_2 + H_2O$) and chromium etchant ($K_3[Fe(CN)_6] + NaOH + H_2O$), respectively. Acetone is used to strip off the PPR. Finally, the wafer is cleaned in isopropyl alcohol and dried with nitrogen spray. The schematic of process flow for fabrication of microelectrodes is depicted in Fig. 8.

3.2 Fabrication of microchannels

In this section, fabrication of microchannels is described. The process of piranha cleaning and deposition of chromium and gold is similar to above mentioned procedure. Photolithography is carried out using mask containing microchannel structures. The metal etching procedure is the one explained above. Channels are then etched in the borofloat substrate using wet or dry etching methods. Fluidic and electrical ports are drilled using water jet cutting machine (OMAX Corporation, Kent, WA, USA). The schematic of process flow for fabrication of microchannels is depicted in Fig. 10.
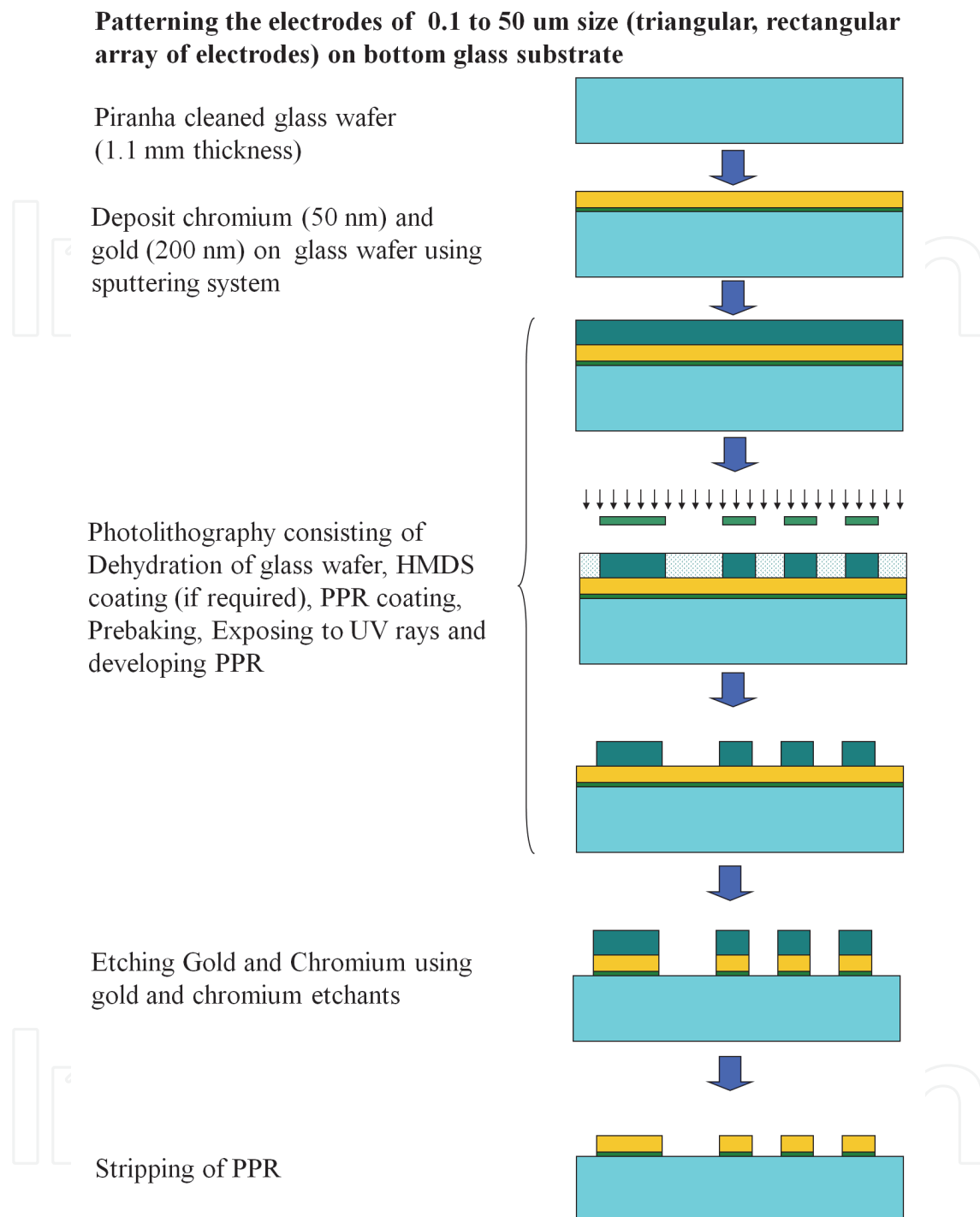
Patterning the electrodes of 0.1 to 50 um size (triangular, rectangular array of electrodes) on bottom glass substrate

Piranha cleaned glass wafer
(1.1 mm thickness)

Deposit chromium (50 nm) and
gold (200 nm) on glass wafer using
sputtering system

Photolithography consisting of
Dehydration of glass wafer, HMDS
coating (if required), PPR coating,
Prebaking, Exposing to UV rays and
developing PPR

Etching Gold and Chromium using
gold and chromium etchants

Stripping of PPR

Fig. 8. Process flow for fabrication of microelectrodes

3.3 Bonding of two substrates

The above fabricated substrates are bonded using fusion process to form a closed channel. The schematic of bonded dielectrophoretic microfluidic chip is shown in Fig. 10. Several layouts of chips on glass wafer are diced using a diamond touch dicing saw.

Microchannels with fluid and electrical access ports in the top glass substrate

Piranha cleaned glass wafer
(1.1 mm thickness)

Deposit chromium (50 nm) and
gold (200nm) on glass wafer using
sputtering system

Photolithography consisting of
Dehydration of glass wafer, HMDS coating
(if required), PPR deposition, Prebaking,
Exposing to UV rays and developing PPR

Dry etching of glass wafer (which will
produce vertical side walls for microchannel)

Stripping of PPR and then etching the
gold and chromium

Fluid and electric access ports will be
produced using water-jet cutter

Fig. 9. Process flow for fabrication of microchannels

Bonding of top and bottom glass substrates using
fusion process

Fig. 10. Schematic of bonded dielectrophoretic microfluidic chip

3.4 Test equipment

Testing of the fabricated device under the influence of DEP phenomena requires AC
voltage source generating four phases, high frequency and high voltage sinusoidal signal.
Instruments like arbitrary waveform generator and voltage amplifier are used to generate
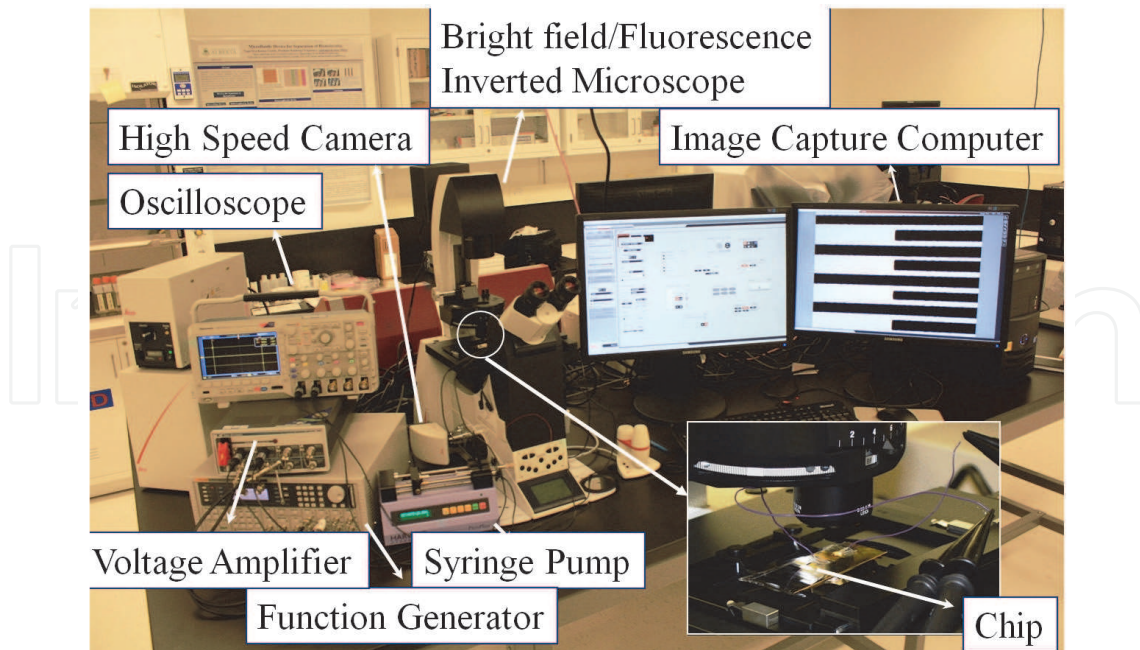
Fig. 11. Testing set-up for DEP experiments

the required AC signals and oscilloscope to check the generated signal for verification. A syringe pump is used to inject the sample into the device. A fully automated bright field and /or fluorescence inverted microscope with high speed monochrome camera is used to observe and capture the process of mixing and separation. The images captured at the detection site of the device are used to quantify the concentration of particles from image processing analysis. The experimental testing set-up discussed above is presented in Fig. 11. The specification and other details of fluidic and electrical connections used in this work can be found in Gunda & Mitra (2010a).

3.5 Experimental results
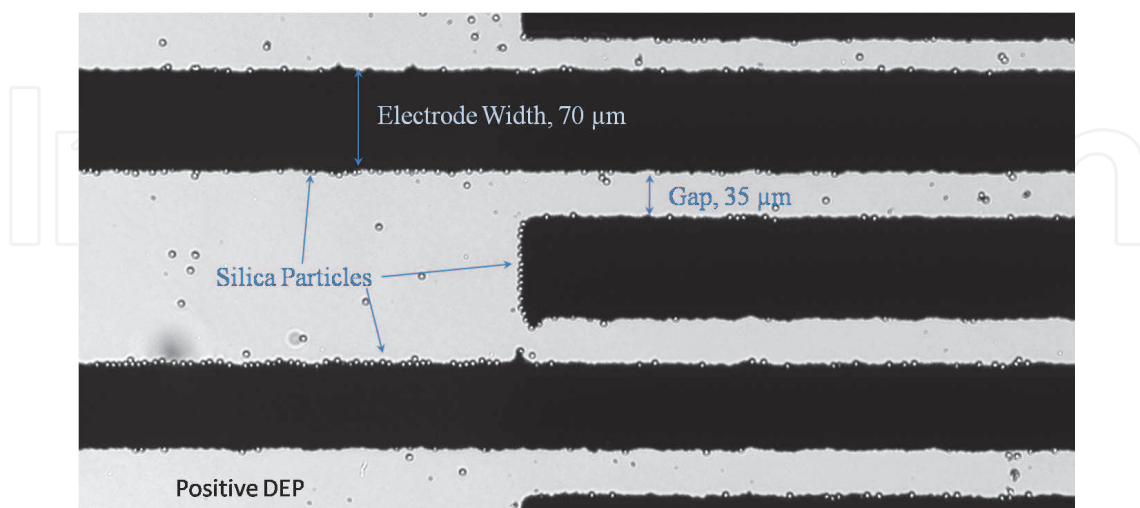
Fig. 12. Positive DEP effect on silica particles

In this section, the results of DEP effects on silica particles are presented. Silica particles of 5 μ diameter are used for these experiments. Both types of DEP effects (positive and negative) are
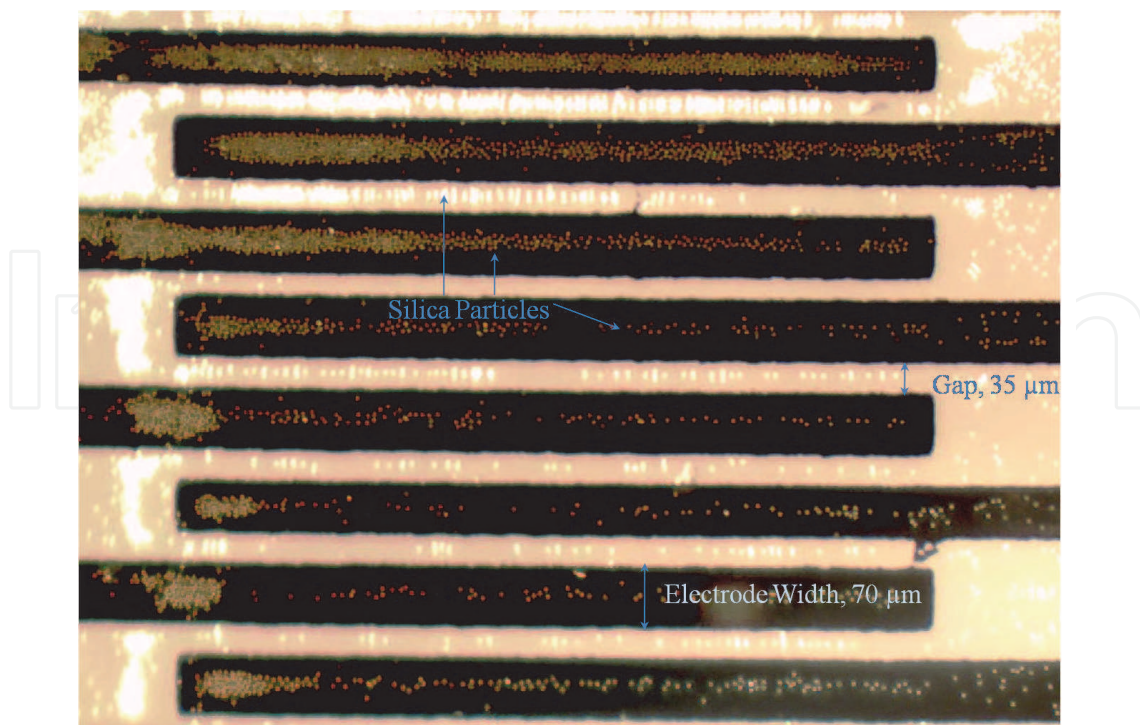
Fig. 13. Negative DEP effect on silica particles

observed for silica particles. Figure 12 shows the positive DEP effect of silica particles under $5 - 10\ V$ applied voltage and for the frequency range of 0 to 1 KHz. It is clearly observed that the particles are trapped at the electrode edges. The image is acquired from the inverted microscope where the light source is placed at the top and a capturing camera is placed at the bottom of the chip. Figure 13 shows the negative DEP effect of silica particles under 10 V applied voltage for the frequency range of 10 KHz to 40 KHz. Under negative effects, the particles move from edges of the electrodes to the middle of the electrodes, to the mid-point of the gap between the electrodes. The spreading of the particles on the electrode surface is also observed when the frequency is shifted from 40 KHz to 60 KHz.

4. Conclusion

Mathematical models for dielectrophoretic transport of bioparticles in a microchannel have been developed. Experiments have been carried out to demonstrate the manipulation of silica particles using DEP. Positive and negative DEP effects on silica particles have been identified.

5. Acknowledgment

6. References

Basuray, S. & Chang, H.-C. (2010). Designing a sensitive and quantifiable nanocolloid assay with dielectrophoretic crossover frequencies, *Biomicrofluidics* 4(1): 013205.

Bunthawin, S., Wanichapichart, P., Tuantranont, A. & Coster, H. G. L. (2010). Dielectrophoretic spectra of translational velocity and critical frequency for a spheroid in traveling electric field, *Biomicrofluidics* 4(1): 014102.

Castellarnau, M., Errachid, A., Madrid, C., Juarez, A. & Samitier, J. (2006). Dielectrophoresis as a tool to characterize and differentiate isogenic mutants of escherichia coli, *Biophys J* 91: 3937–3945.

Chang, D. E., Loire, S. & Mezic, I. (2003). Closed-form solutions in the electrical field analysis for dielectrophoretic and travelling wave inter-digitated electrode arrays, *J Phys D: Appl Phys* 36: 3073–3078.

Church, C., Zhu, J., Wang, G., Tzeng, T.-R. J. & Xuan, X. (2009). Electrokinetic focusing and filtration of cells in a serpentine microchannel, *Biomicrofluidics* 3(4): 044109.

Clague, D. S. & Wheeler, E. K. (2001). Dielectrophoretic manipulation of macromolecules: The electric field, *Phys Rev E: Stat Nonlinear Soft Matter Phys* 64: 026605.

Crews, N., Darabi, J., Voglewede, P., Guo, F. & Bayoumi, A. (2001). An analysis of interdigitated electrode geometry for dielectrophoretic particle transport in micro-fluidics, *Scand J Clin Lab Invest* 61: 95–102.

Du, J.-R., Juang, Y.-J., Wu, J.-T. & Wei, H.-H. (2008). Long-range and superfast trapping of dna molecules in an ac electrokinetic funnel, *Biomicrofluidics* 2(4): 044103.

Ferrier, G. A., Hladio, A. N., Thomson, D. J., Bridges, G. E., Hedayatipoor, M., Olson, S. & Freeman, M. R. (2008). Microfluidic electromanipulation with capacitive detection for the mechanical analysis of cells, *Biomicrofluidics* 2(4): 044102.

Gagnon, Z., Mazur, J. & Chang, H.-C. (2009). Glutaraldehyde enhanced dielectrophoretic yeast cell separation, *Biomicrofluidics* 3(4): 044108.

Green, N. G., Ramos, A. & Morgan, H. (2002). Numerical solution of the dielectrophoretic and traveling wave forces for interdigitated electrode arrays using the finite element method, *Journal of Electrostatics* 56: 235–254.

Gunda, N. S. K. & Mitra, S. K. (2009). Modeling of dielectrophoresis for myoglobin molecules in a microchannel with parallel electrodes, Proceedings of the ASME 2009 International Mechanical Engineering Congress and Exposition, Lake Buena Vista, Florida, USA, November 13-19, IMECE2009-10765.

Gunda, N. S. K. & Mitra, S. K. (2010a). Experimental investigation of dielectrophoretic behaviour of myoglobin and silica particles on a microelectrode chip, Proceedings of ASME 2010 3rd Joint USEuropean Fluids Engineering Summer Meeting and 8th International Conference on Nanochannels, Microchannels, and Minichannels, Montreal, Canada, August 2-4, FEDSM-ICNMM2010- 30306.

Gunda, N. S. K. & Mitra, S. K. (2010b). Modeling of dielectrophoretic transport of myoglobin molecules in microchannels, Biomicrofluidics 4(1): 014105.

Gunda, N. S. K., Mitra, S. K. & Bhattacharjee, S. (2009). Dielectrophoretic mixing with novel electrode geometry, Proceedings of the ASME 2009 Fluids Engineering Division SummerMeeting, FEDSM09, Vail, Colorado, August 2-6, FEDSM2009-78260.

Gunda, N. S. K., Mitra, S. K. & Rao, V. R. (2009). Fabrication of dielectrophoretic microfluidic Device, Proceedings of the Seventh International ASME Conference on Nanochannels, Microchannels and Minichannels, Pohang, South Korea, June 22-24, ICNMM2009-82170.

Hughes, M. P. (2003). *Nanoelectromechanics in Engineering and Biology*, CRC Press, Boca Raton.

Hwang, H., Lee, D.-H., Choi, W. & Park, J.-K. (2009). Enhanced discrimination of normal oocytes using optically induced pulling-up dielectrophoretic force, *Biomicrofluidics* 3(1): 014103.

Jones, T. B. (1995). *Electromechanics of particles*, Cambridge University Press.

Lewpiriyawong, N., Yang, C. & Lam, Y. C. (2008). Dielectrophoretic manipulation of particles in a modified microfluidic h filter with multi-insulating blocks, *Biomicrofluidics* 2(3): 034105.

Lin, J. T. Y. & Yeow, J. T. W. (2007). Enhancing dielectrophoresis effect through novel electrode geometry, *Biomed Microdevices* 9(6): 823–831.

Manuel, G. & Clague, D. (2000). The 2d electric field above a planar sequence of independent strip electrodes, *J Phys D: Appl Phys* 33: 1747–1755.

Masliyah, J. & Bhattacharjee, S. (2006). *Electrokinetic and Colloid Transport Phenomena*, Willey Interscience, Hoboken, New Jersey.

Molla, S. H. & Bhattacharjee, S. (2005a). Prevention of colloidal membrane fouling employing dielectrophoretic forces on a parallel electrode array, *J Membr Sci* 255: 187–199.

Molla, S. H. & Bhattacharjee, S. (2005b). Simulations of a dielectrophoretic membrane filtration process for removal of water droplets from water-in-oil emulsions, *J Colloid Interface Sci* 287: 338–350.

Molla, S. H. & Bhattacharjee, S. (2007). Dielectrophoretic leviation in the presence of shear flow: Implications for colloidal fouling of filtration membranes, *Langmuir* 23(21): 10618–10627.

Morgan, H., Alberto, G. I., David, B., Green, N. G. & Ramos, A. (2001). The dielectrophoretic and traveling wave forces generated by interdigited electrode arrays: Analytical solution using fourier series, *J Phys D: Appl Phys* 34: 1553–1561.

Nguyen, N. T. & Werely, S. T. (2006). *Fundamentals and Applications of Microfluidics*, Artech House, Boston.

Parikesit, G. O. F., Markesteijn, A. P., Piciu, O. M., Bossche, A., Westerweel, J., Young, I. T. & Garini, Y. (2008). Size-dependent trajectories of dna macromolecules due to insulative dielectrophoresis in submicrometer-deep fluidic channels, *Biomicrofluidics* 2(2): 024103.

Pohl, H. A. (1978). *Dielectrophoresis*, Cambridge University Press.

Wang, X. B., Huang, Y., Burt, J. P. H., Markx, G. H. & Pethig, R. (1993). Selective dielectrophoretic confinement of bioparticles in potential energy wells, *J Phys D: Appl Phys* 26: 1278–1285.

Wang, X., Wang, X. B., Becker, F. F. & Gascoyne, R. C. P. (1996). A theoretical method of electric field analysis for dielectrophoretic electrode arrays using green's theorem, *J Phys D: Appl Phys* 29: 1649–1660.

Wei, M.-T., Junio, J. & Ou-Yang, H. D. (2009). Direct measurements of the frequency-dependent dielectrophoresis force, *Biomicrofluidics* 3(1): 012003.

Yang, C. Y. & Lei, U. (2007). Quasistatic force and torque on ellipsoidal particles under generalized dielectrophoresis, *J Appl Phys* 102: 094702.

Yang, F., Yang, X., Jiang, H., Bulkhaults, P., Wood, P., Hrushesky, W. & Wang, G. (2010). Dielectrophoretic separation of colorectal cancer cells, *Biomicrofluidics* 4(1): 013204.

Zhu, X., Yi, H. & Ni, Z. (2010). Frequency-dependent behaviors of individual microscopic particles in an optically induced dielectrophoresis device, *Biomicrofluidics* 4(1): 013202.
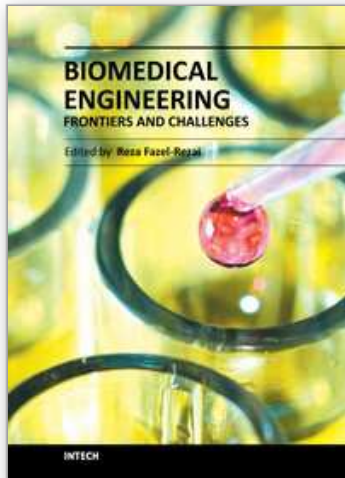
Biomedical Engineering - Frontiers and Challenges

Edited by Prof. Reza Fazel

In all different areas in biomedical engineering, the ultimate objectives in research and education are to improve the quality life, reduce the impact of disease on the everyday life of individuals, and provide an appropriate infrastructure to promote and enhance the interaction of biomedical engineering researchers. This book is prepared in two volumes to introduce recent advances in different areas of biomedical engineering such as biomaterials, cellular engineering, biomedical devices, nanotechnology, and biomechanics. It is hoped that both of the volumes will bring more awareness about the biomedical engineering field and help in completing or establishing new research areas in biomedical engineering.

How to reference

In order to correctly reference this scholarly work, feel free to copy and paste the following:

Naga Siva K. Gunda and Sushanta K. Mitra (2011). Dielectrophoresis for Manipulation of Bioparticles, Biomedical Engineering - Frontiers and Challenges, Prof. Reza Fazel (Ed.), ISBN: 978-953-307-309-5, InTech, Available from: http://www.intechopen.com/books/biomedical-engineering-frontiers-and-challenges/dielectrophoresis-for-manipulation-of-bioparticles

INTECH
open science | open minds